


## Article

# Experimental Study on the Impact of CO<sub>2</sub> Treatment on Different Lithofacies in Shale Oil Reservoirs

Jiaping Tao <sup>1,2</sup> , Siwei Meng <sup>2</sup>, Dongxu Li <sup>3</sup>, Gang Cao <sup>2</sup>, Yang Gao <sup>2</sup> and He Liu <sup>1,2,\*</sup>

<sup>1</sup> School of Petroleum Engineering, China University of Petroleum (East China), Qingdao 266580, China; taojiaping93@sina.com

<sup>2</sup> PetroChina Research Institute of Petroleum Exploration & Development, Beijing 100083, China; mengsw@petrochina.com.cn (S.M.); caogang1972@petrochina.com.cn (G.C.); gaoyang573@petrochina.com.cn (Y.G.)

<sup>3</sup> PetroChina Daqing Oilfield Co., Ltd., Daqing 163002, China; ldongxu@petrochina.com.cn

\* Correspondence: liuhe@petrochina.com.cn

**Abstract:** CO<sub>2</sub> technology has been progressively used in the development of shale oil. After injection, CO<sub>2</sub> can react with formation water to form carbonic acid, which then reacts with carbonate and silicate minerals, resulting in changes in porosity and permeability. However, there are some debates as to whether the effect of CO<sub>2</sub> improves or damages porosity and permeability. So, in this paper, systematic experiments were carried out to clarify the interaction between CO<sub>2</sub> and shale in different lithofacies and to draw a pertinent conclusion. The results showed that the shale in Qingshankou Formation could be divided into three main lithofacial types: foliaceous shale, laminated feisic shale and laminated diamictic shale. There were relatively more pores, some natural microfractures and small mineral particles in foliaceous shale, a few micropores and large mineral particles in laminated feisic shale, some biogenic calcium carbonate minerals and hardly any micropores in laminated diamictic shale. Due to the diversity of micromorphology and mineral composition, the effects of CO<sub>2</sub> treatment had significant differences. For foliaceous shale, CO<sub>2</sub> treatment had both improving and damaging effects on porosity and permeability; for laminated shale, both porosity and permeability improved significantly. So, it is necessary to identify the main lithofacies of target formation before the application of CO<sub>2</sub> technology in shale oil reservoirs.

**Keywords:** shale oil; lithofacies; CO<sub>2</sub> treatment; micromorphology; porosity and permeability



**Citation:** Tao, J.; Meng, S.; Li, D.; Cao, G.; Gao, Y.; Liu, H. Experimental Study on the Impact of CO<sub>2</sub> Treatment on Different Lithofacies in Shale Oil Reservoirs. *Appl. Sci.* **2022**, *12*, 2217. <https://doi.org/10.3390/app12042217>

Academic Editor: Arcady Dyskin

Received: 20 January 2022

Accepted: 15 February 2022

Published: 21 February 2022

**Publisher's Note:** MDPI stays neutral with regard to jurisdictional claims in published maps and institutional affiliations.



**Copyright:** © 2022 by the authors. Licensee MDPI, Basel, Switzerland. This article is an open access article distributed under the terms and conditions of the Creative Commons Attribution (CC BY) license (<https://creativecommons.org/licenses/by/4.0/>).

## 1. Introduction

Unconventional oil and gas are the current focuses of oil and gas exploration and development; among them, shale oil is the most strategic replacement resource, with huge development potential [1–3]. Restricted by ultra-low porosity and permeability, shale oil reservoirs are facing the problem of rapid production decline in the process of development. The oil recovery factor of shale oil is less than 10%, generally, which is much lower than the average recovery factor of conventional crude oil [4–7]. In order to slow down the production decay rate and obtain higher oil recovery, it is urgent to explore enhanced oil recovery technology for shale oil.

The ultra-low porosity and permeability of shale oil reservoirs restrict the application of conventional EOR technologies [8–10]. On the basis of laboratory experiments and numerical simulation studies, researchers find that huff-and-puff gas injection and surfactant imbibition are the most feasible enhanced oil recovery methods for shale oil [11–14]. CO<sub>2</sub> injection technology can effectively improve oil recovery through the mechanisms of miscible flooding, viscosity reduction and formation energy supplements, and has received extensive attention from researchers [15–19].

After being injected into a formation, CO<sub>2</sub> can react with formation water to form carbonic acid, which can react with carbonate and silicate minerals in the shale, resulting

in changes in reservoir porosity and permeability. However, CO<sub>2</sub> has both positive and negative effects on reservoir porosity and permeability after complex reactions [20–24]. On the one hand, these reactions can dissolve part of the matrix minerals, increasing the matrix porosity effectively. Additionally, this dissolution can increase the size of the seepage channel and improve the pore connectivity, thereby increasing the permeability of shale oil reservoirs. On the other hand, new mineral precipitation will be produced after the interactions between CO<sub>2</sub> and minerals, such as potassium feldspar, albite and chlorite. Additionally, the dissolution of cement causes the migration of mineral particles. Both the precipitation and migration of minerals may block pores and throats and reduce matrix porosity. Furthermore, these cause a decrease in pore connectivity and damage the permeability of shale oil reservoirs.

There are strong vertical heterogeneity and mineral composition differences in the continental shale oil reservoirs of China [25–28]. So, the changes in porosity and permeability in different formations are significantly different after CO<sub>2</sub> injection. Therefore, it is necessary to carry out systematic experiments to clarify the interaction between CO<sub>2</sub> and shale in different lithofacies, and its effect on the porosity and permeability of shale oil reservoirs. In this paper, the main lithofacial types of the target formation are identified through core observation and X-ray fluorescence (XRF) spectrum analysis. Then, shale samples in different lithofacies are selected for CO<sub>2</sub> soaking experiments. Finally, the influence of CO<sub>2</sub> treatment on shale is explored by X-ray diffraction (XRD) mineral composition analysis, scanning electron microscope (SEM) micromorphology analysis and characterizations of porosity and permeability.

## 2. Materials and Methods

### 2.1. Sample Preparation

Our shale samples are from the Qingshankou Formation in the Songliao Basin (Figure 1), which is one of China's most important continental shale oil reservoirs. The Songliao Basin is located in northeast China, and the Qingshankou Formation in this basin develops high quality shales in which extensive hydrocarbon has been shown. The geological resources in this formation are about  $54.6 \times 10^8$  t and have huge exploration and development potential. The reservoir of the Qingshankou Formation is mainly shale, with a few sandstone and limestone interbeds, and the formation depth is about 1500–2500 m. The content of brittle minerals is high, and the proportion of clay minerals is 30–60%. The ionic composition of the brine used in the following experiments is shown in Table 1, measured from the produced water.

The shale samples are processed into small pieces and huge bulk samples by mechanical cutting. Then, the cut surfaces of these bulk samples are polished by an automatic polish–grinding machine. After polishing, the bulk samples are put into an ultrasonic cleaner to remove contaminants and keep the cut surface of these samples flat and clean. These processed small pieces and huge bulk samples are shown in Figure 2a,b.

The SEM samples are cut from target areas of huge bulk samples and the size of these samples is 0.5 cm × 1 cm × 1 cm, processed by mechanical cutting. Then, the SEM samples are fixed to sample holders and their top surfaces are polished with sandpaper. After mechanical polishing, the samples are put into an argon ion polisher for 4 hours' processing. Finally, the polished samples are plated with a thin layer of carbon on their surfaces. SEM samples are shown in Figure 2c.

The shale samples are processed into core samples by numerically controlled wire cutting, and the size of these core samples is 25 mm in diameter and 50 mm in length. After processing, those core samples that have retained their integrity, have no damage and are fracture-free are chosen and polished with sandpaper to keep their surfaces smooth and their end surfaces flat. Then these samples are put into an oil-cleaning instrument for one week to clean off the crude oil and ensure the samples are clean and damage-free. Processed core samples are shown in Figure 2d and the direction of these samples is parallel to the bedding.

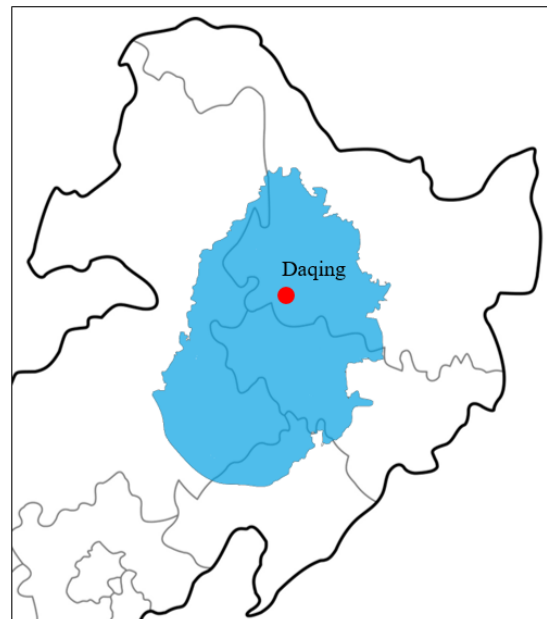


**Figure 1.** Geographical location of shale samples collection sites.

**Table 1.** Ionic composition of the brine.

Ion	Na <sup>+</sup> and K <sup>+</sup>	Ca <sup>2+</sup>	Mg <sup>2+</sup>	Cl <sup>-</sup>	SO <sub>4</sub> <sup>2-</sup>	HCO <sub>3</sub> <sup>-</sup>
concentration (mg/L)	2320	39	5	1450	307	3420

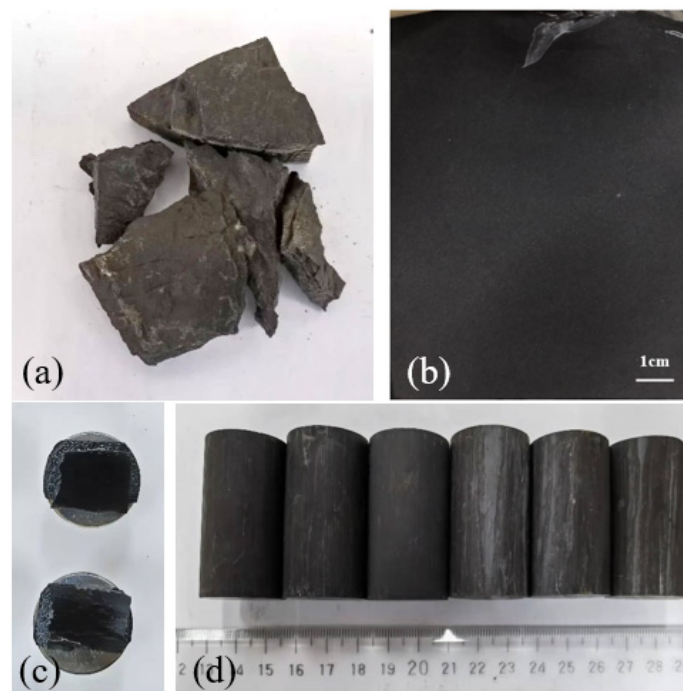


**Figure 2.** Photos of the processed samples: (a) crushed samples; (b) bulk samples; (c) SEM samples and (d) core samples.

## 2.2. Experimental Apparatus and Methods

### 2.2.1. Experimental Apparatus

The element distribution in a large area of each shale sample is measured through the XRF analysis using an M4 TORNADO X-ray fluorescence spectrometric instrument from Bruker, Germany. In this experiment, the area scan method is adopted and the vacuum degree, voltage and current are kept at 20 mbar, 50 kV and 200  $\mu$ A, respectively.

The pore structures and micromorphologies of the shale samples are measured through SEM analysis, using an Apreo field-emission scanning electron microscopy from ThermoFisher Scientific, USA. The instrument's maximum resolution is 1 nm under 1 kV. In this experiment, the work distance, voltage and current are kept at 10 mm, 10 kV and 1.6 nA, respectively.

The mineral composition of shale samples is measured through XRD analysis using D/max 2500 PC X-ray diffractometer from Rigaku Corporation, Japan. In this experiment, the average particle size of shale samples is 125–150  $\mu$ m, and the scanning angle is 3–85° at a scanning speed of 1°/min. The detailed procedures can be found in SY/T5163-2010.

The porosity and permeability of shale samples are measured with helium before and after CO<sub>2</sub> treatment, using an AP-608 Automated Permeameter-Pososimeter from Coretest systems, USA. The maximum confining pressure is 9000 psi and the measuring range of porosity and permeability are 0.1–40% and 0.001–10000 mD, respectively.

### 2.2.2. Experimental Methods

A schematic depiction of the CO<sub>2</sub> treatment apparatus used in this research is shown in Figure 3. The apparatus mainly consists of an ISCO pump, a pressure gauge, two intermediate containers and a vacuum pump. The experimental procedures of SEM and XRD analysis, before and after CO<sub>2</sub> treatment, are briefly described as follows. Firstly, the micromorphology and mineral composition of shale are measured through SEM and XRD analysis, respectively. Next, the samples and CO<sub>2</sub>-saturated brine are put into a clean intermediate container for CO<sub>2</sub> treatment. The temperature and pressure of CO<sub>2</sub> treatment are set at 90 °C and 30 MPa. Finally, after 7 days of treatment, the samples are taken out and dried in an oven, and subsequently are subject to characterization of micromorphology and mineral composition to analyze the influences of CO<sub>2</sub> treatment.

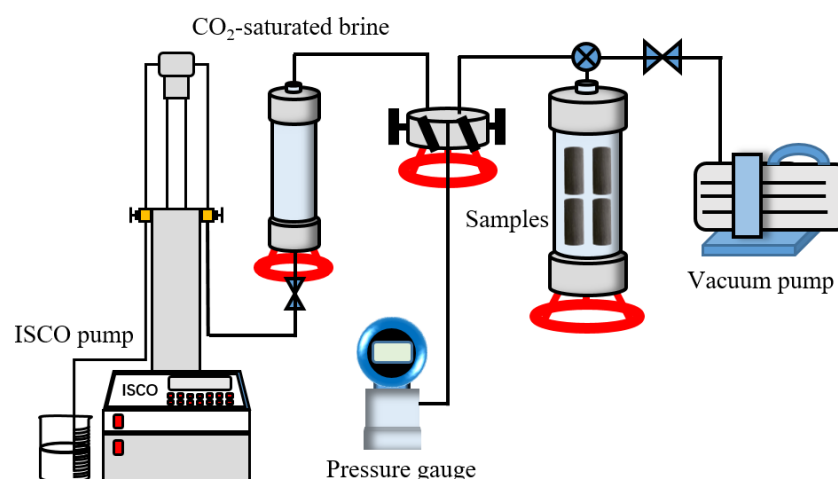


**Figure 3.** Schematic depiction of the experimental setup for CO<sub>2</sub> treatment.

The experimental procedures of porosity and permeability analysis before and after CO<sub>2</sub> treatment are briefly described as follows. Firstly, the porosity and permeability of shale are measured with a permeameter–porosimeter. Next, the core samples are put into a clean intermediate container and soaked in CO<sub>2</sub>-saturated brine for the periods of 1 day, 3 days, 5 days or 7 days, after which they are dried and subjected to porosity and permeability analysis to analyze the influences of different CO<sub>2</sub> treatment times.

### 3. Results and Discussion

#### 3.1. Lithofacies Analysis of Qingshankou Formation

The main lithofacial types of the Qingshankou Formation are identified through core observation and XRF analysis, and the results are shown in Figure 4. The shale in the Qingshankou Formation can be divided into three main lithofacial types: foliaceous shale, laminated feisic shale and laminated diamictic shale. These three main types of shale account for more than 90% of the Qingshankou formation and are the main target area for exploration and development.

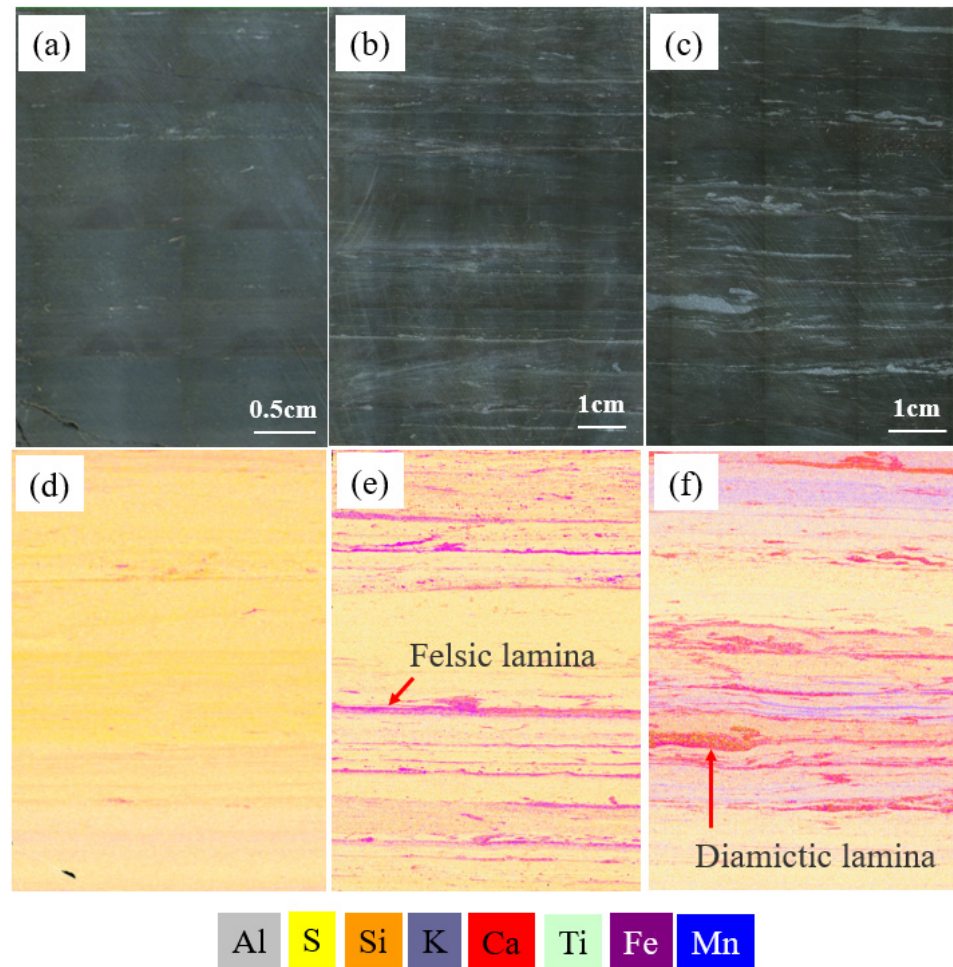


**Figure 4.** Results of core observation and XRF analysis: (a) photo of foliaceous shale; (b) photo of laminated feisic shale; (c) photo of laminated diamictic shale; (d) element distribution of foliaceous shale; (e) element distribution of laminated feisic shale and (f) element distribution of laminated diamictic shale.

The photo and XRF result of foliaceous shale sample are shown in Figure 4a,d. The foliaceous shale is mainly black and dark gray, with a fine texture, high oil saturation and low interlayer difference. Its element distribution is relatively uniform. The photo and XRF result of laminated feisic shale sample are shown in Figure 4b,e. The laminated feisic shale is mainly dark gray with relatively low oil saturation and significant interlayer difference. Its element distribution is uneven with many feisic laminas. The thickness of these laminas is about 1 mm and their composition is mainly silica and iron elements, indicating a rapid alternative change of highly organic shale and lowly organic silty laminas. The photo and XRF result of laminated diamictic shale sample are shown in Figure 4c,f. The laminated diamictic shale is mainly dark gray with relatively low oil saturation and significant interlayer difference. Its element distribution is uneven, with many diamictic

laminae. The thickness of these laminae is about 1 mm and their compositions are mainly silica, iron and calcium elements, indicating a rapid alternative change from highly organic shale to lowly organic silty and carbonate laminae.

The average mineral composition of these three main types of shale is shown in Figure 5. The results show that the main minerals of foliaceous shale are clay minerals, quartz and feldspar. Clay minerals account for more than half of the total mineral content, and the proportions of quartz and feldspar are 27.4% and 10.8%, respectively. The proportions of carbonate and other minerals are very low, only 5.3% and 3.3%, respectively. For laminated felsic shale, quartz and feldspar together account for about half of the total minerals and are greater than the proportion of clay minerals, which is 41.9%. The proportion of carbonate and other minerals is very low, less than 5%. For laminated diamictic shale, quartz and feldspar together account for 41.6% of the total minerals and are greater in proportion than that of clay minerals, which is 40.3%. The proportion of carbonate minerals is relatively high and accounts for more than 15% of the total content. Obviously, there are significant differences in the mineral composition among these three main types of shale samples.

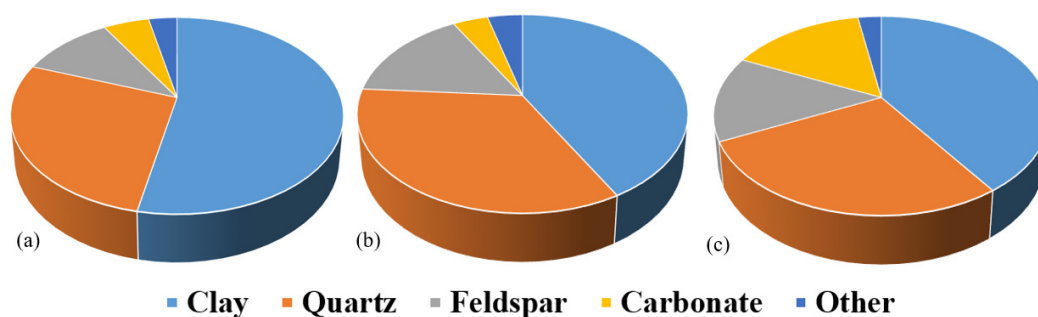


**Figure 5.** Average mineral composition of shale samples: (a) foliaceous shale; (b) laminated felsic shale; and (c) laminated diamictic shale.

Due to the significant differences of mineral composition, varied micromorphologies and pore structures are observed during SEM analysis and the results are shown in Figure 6. As shown in Figure 6a,b, after mechanical and argon ion polishing, the micromorphologies of foliaceous shale samples are smooth, flat and tight. There are some micropores, the sizes of which are less than 5  $\mu\text{m}$ . The main reservoir spaces are micro fractures, intergranular pores and organic pores. The number and size of these pores are relatively many and large, with some natural microfractures. As a result, the connectivity between pores and fractures maybe good, which may form seepage networks for shale oil. The micromorphology of laminated felsic shale is tighter than foliaceous shale and has only a few micropores, the sizes of which are less than 3  $\mu\text{m}$ . The main reservoir spaces are intergranular pores, granular dissolved pores and intergranular fractures. The number and size of these pores are fewer and smaller, with few natural microfractures. As a result, the connectivity between pores and fractures is poor, and it is difficult for shale oil to flow. The micromorphology of laminated diamictic shale is tightest among the three types of shale, and there are hardly any micropores. The main reservoir spaces are intergranular pores, granular dissolved pores and intergranular fractures. Due to diagenetic cementation, the number and sizes of these pores and fractures are few and small. As a result, the connectivity between pores and fractures is least, through which it is difficult for shale oil to flow. In addition, there are many biogenic calcium carbonate minerals that cannot be observed in other samples. The differences in micromorphologies and pore structures may affect the results of the  $\text{CO}_2$  treatment.

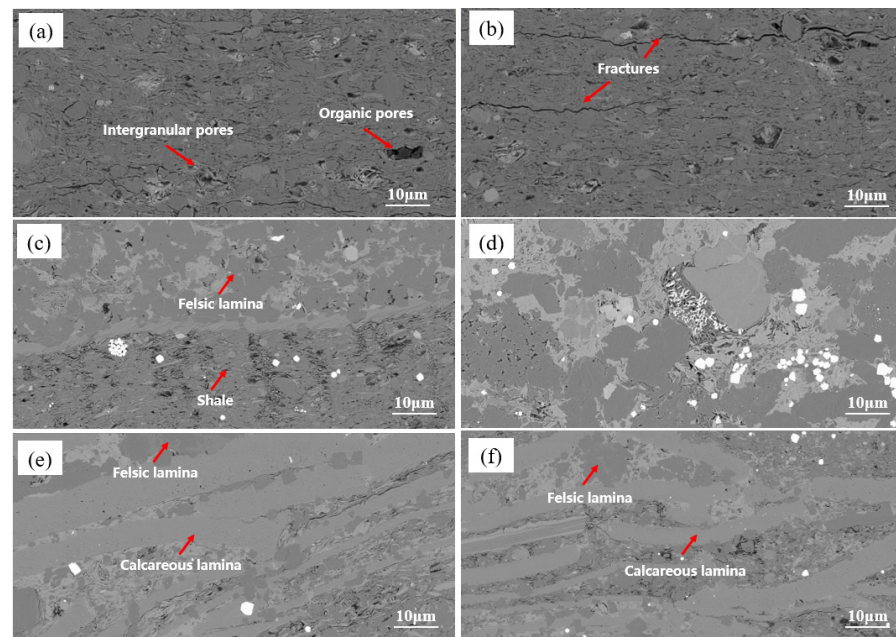
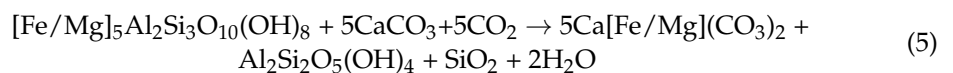
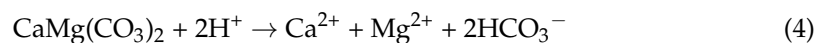
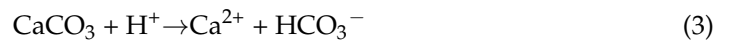
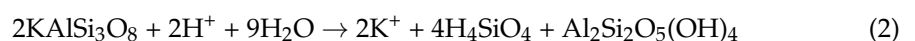
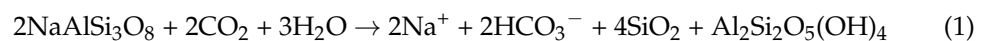


**Figure 6.** SEM analysis of shale samples: (a,b) foliaceous shale; (c,d) laminated felsic shale and (e,f) laminated diamictic shale.

### 3.2. Micromorphology Analysis on Different Lithofacial Types of Shale during CO<sub>2</sub> Treatment

In order to explore the effect of CO<sub>2</sub> treatment on the micromorphologies of different lithofacial types of shale, SEM analysis is carried out and the results are shown in Figure 7. The original pore structures and micromorphologies of foliaceous shale are shown in Figure 7a. After mechanical and argon ion polishing, the surfaces of the shale samples become smooth and tight, without mineral migration. There are a few small primary pores, and the pore connectivity is poor. After CO<sub>2</sub> treatment, the CO<sub>2</sub>–water–rock reaction significantly affects the surface structures of the shale samples, and many new dissolution pores are generated, as shown in Figure 7d. According to the XRD analysis, the main minerals of the shale samples are albite, potash feldspar, calcite, dolomite and chlorite, and the probable interaction mechanism during CO<sub>2</sub> treatment is shown as follows:



Due to the small size and scattered distribution of mineral particles, the sizes of new dissolution pores are small and the improvement in pore connectivity is poor. Meanwhile, CO<sub>2</sub> treatment results in some new mineral precipitation and migration by geochemical reactions. Both the precipitation and migration of minerals block pores and throats and reduce the porosity and pore connectivity of shale samples, leading to a decrease in permeability.

The original pore structures and micromorphologies of laminated felsic shale are shown in Figure 7b. The surfaces of the shale samples are smooth and tight, without mineral migration. There are a few small primary pores, and the pore connectivity is poor. After CO<sub>2</sub> treatment, the CO<sub>2</sub>–water–rock reaction significantly leads to many new dissolution pores, as shown in Figure 7e. In certain areas, rich in albite, potash feldspar, calcite and so forth, large-scale dissolution of these minerals occurs and results in many

large-sized pores. Due to the large sizes of mineral particles in laminas, the sizes of new dissolution pores can reach 10–30  $\mu\text{m}$  in diameter. Although the precipitation and migration of minerals caused by  $\text{CO}_2$  treatment partially block pores and throats, the porosity and pore connectivity of the shale samples is still improved significantly under the existence of large-sized dissolution pores, leading to an increase in permeability.

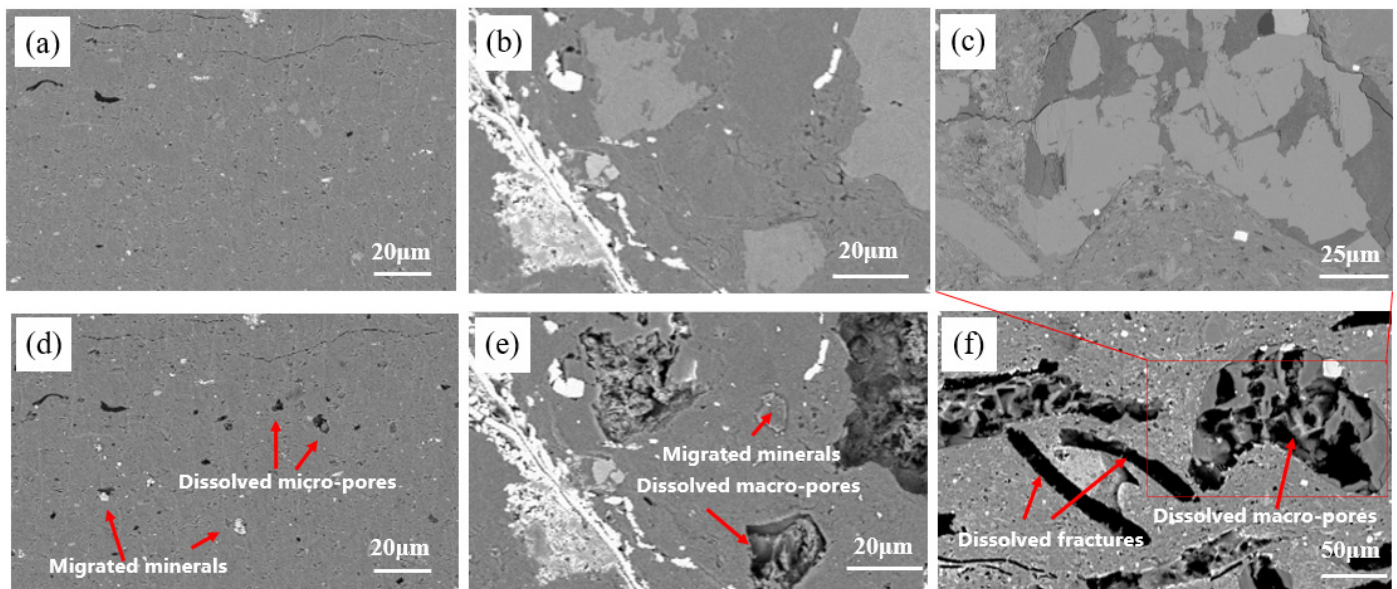


**Figure 7.** SEM analysis results before and after  $\text{CO}_2$  treatment: (a) foliaceous shale before treatment; (b) laminated feisic shale before treatment; (c) laminated diamictic shale before treatment; (d) foliaceous shale after treatment; (e) laminated feisic shale after treatment and (f) laminated diamictic shale after treatment.

The original pore structures and micromorphologies of laminated diamictic shale are shown in Figure 7c. The surface of the shale samples becomes smooth and tight, without mineral migration. Due to the fine diagenetic cementation, there are hardly any micropores, and the pore connectivity is poor. After  $\text{CO}_2$  treatment, the  $\text{CO}_2$ –water–rock reaction significantly leads to many new dissolution pores, as shown in Figure 7f. There is a large-scale dissolution of some minerals, such as albite, potash feldspar, calcite and so forth. Due to the large sizes of mineral particles in laminas, the sizes of new dissolution pores can reach 50  $\mu\text{m}$  in diameter. Furthermore, the dissolution of biogenic calcium carbonate minerals results in many dissolution microfractures, which can significantly improve the porosity and pore connectivity of shale and increase the flowability of shale oil. Although the precipitation and migration of minerals caused by  $\text{CO}_2$  treatment partially block pores and throats, the porosity and pore connectivity of the shale samples is still improved significantly by the presence of large-sized dissolution pores and fractures. So, after  $\text{CO}_2$  treatment, the permeability of shale samples can be improved significantly.

### 3.3. Mineral Composition Analysis of Different Lithofacial Types of Shale during $\text{CO}_2$ Treatment

In order to explore the effect of  $\text{CO}_2$  treatment on the mineral compositions of different lithofacial types of shale, XRD analysis is carried out before and after  $\text{CO}_2$  treatment, and the results are shown in Table 2. Although there are significant differences in mineral composition among these three main types of shale samples, the change rules of mineral composition are similar between them. Compared with the samples without  $\text{CO}_2$  treatment, the proportion of feldspar and carbonate minerals of the treated samples decreases by 4.4–7.2% and 2.8–9.1%, respectively. In combination with SEM analysis, it is revealed that happens because of the dissolution of feldspar and carbonate minerals in the  $\text{CO}_2$  treatment. Quartz does not react with  $\text{CO}_2$  and the increase in its content is caused by the decrease in the overall quality of the shale samples. Meanwhile, as shown in Formulas 1 and 5, albite



and chlorite react with CO<sub>2</sub> to create quartz. As a result, the proportion of quartz increases obviously after CO<sub>2</sub> treatment.

**Table 2.** Mineral composition analysis of shale samples.

Lithofacies	Treatment	Mineral Composition (%)				
		Quartz	Feldspar	Clay	Carbonate	Other
foliaceous shale	untreated	26.6	11.2	52.9	6.1	3.2
	CO <sub>2</sub> treated	34.3	6.8	50.2	3.3	5.4
laminated felsic shale	untreated	31.1	19.3	40.6	4.1	4.9
	CO <sub>2</sub> treated	39.3	12.1	38.9	2.1	7.6
laminated diamictic shale	untreated	28.1	10.8	41.2	16.3	4.6
	CO <sub>2</sub> treated	37.1	5.6	43.2	7.2	6.9

### 3.4. Porosity and Permeability Analysis of Different Lithofacial Types of Shale during CO<sub>2</sub> Treatment

In order to explore the effects of CO<sub>2</sub> treatment on the porosity and permeability of different lithofacial types of shale, core soaking experiments are carried out. The physical properties of the shale core samples are listed in Table 3. Sample Q1 and Q2 are obtained from foliaceous shale formation. Sample Q3 and Q4 are obtained from laminated felsic shale formation. Sample Q5 and Q6 are obtained from laminated diamictic shale formation. As shown in Table 3, the porosities of core samples are extremely low and only 4.56–8.11% under confining pressure conditions. The porosity of foliaceous shale is the highest and the laminated felsic shale ranks the second, which is consistent with the SEM results above. Furthermore, the connectivity of shale is poor, and the permeability of core samples is extremely low and only 0.0417–0.0767 mD, making it difficult for shale oil to flow.

**Table 3.** Physical properties of shale cores.

Sample	Diameter (cm)	Length (cm)	Porosity (%)	Permeability (mD)
Q1	2.50	5.02	8.11	0.0572
Q2	2.51	5.01	7.29	0.0443
Q3	2.51	4.99	6.17	0.0628
Q4	2.50	5.02	5.42	0.0767
Q5	2.52	5.01	5.77	0.0417
Q6	2.51	5.00	4.56	0.0421

The results of porosity and permeability after CO<sub>2</sub> treatment are shown in Figures 8 and 9, and there are significant differences in the change rules for porosity and permeability among the three main types of shale. For foliaceous shale, CO<sub>2</sub> treatment has both improving and damaging effects on porosity and permeability. With the increasing treatment time, the porosity and permeability of Q1 sample show a fluctuating, upward trend. After 7 days' treatment, the porosity and permeability of the Q1 sample increase by 8.14% and 62.93%, respectively. Meanwhile, with the increasing treatment time, the porosity and permeability of the Q2 sample decline noticeably. After 7 days' treatment, the porosity and permeability of the Q2 sample decrease by 13.17% and 63.43%, respectively. In combination with SEM analysis, it is revealed that there are many new, small dissolution pores, and precipitation and migration of minerals occur after CO<sub>2</sub> treatment. When the dissolution effect dominates, CO<sub>2</sub> treatment can improve porosity and permeability significantly (Q1). When the precipitation and migration effects dominate, CO<sub>2</sub> treatment shows a damaging effect on porosity and permeability (Q2). Therefore, serious consideration should be given to potential reservoir damage when CO<sub>2</sub> is injected into foliaceous shale formations.

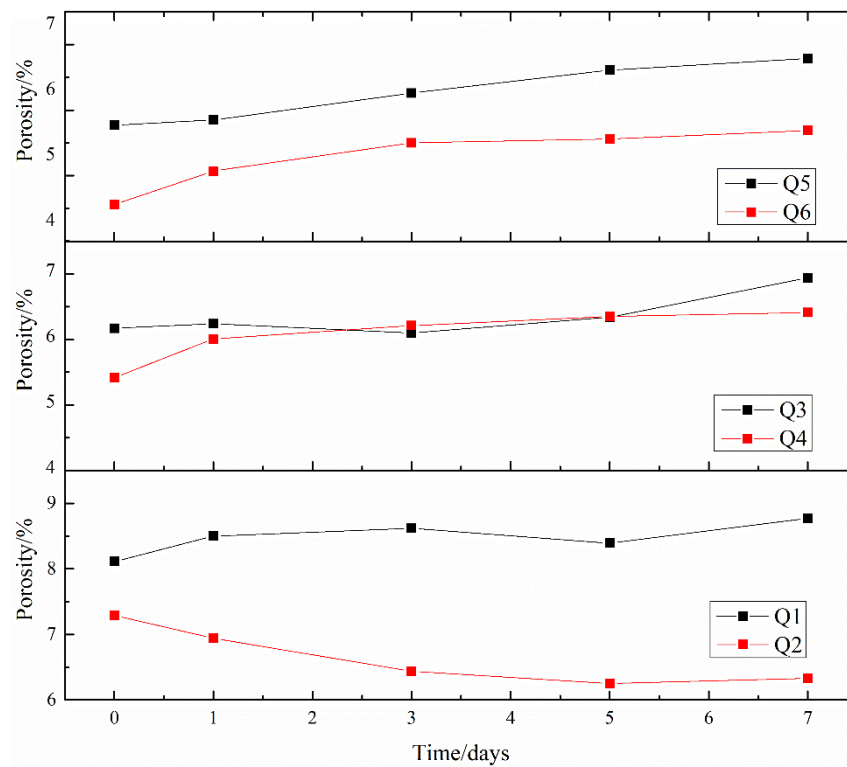


Figure 8. Porosity analysis of shale core samples during CO<sub>2</sub> treatment.

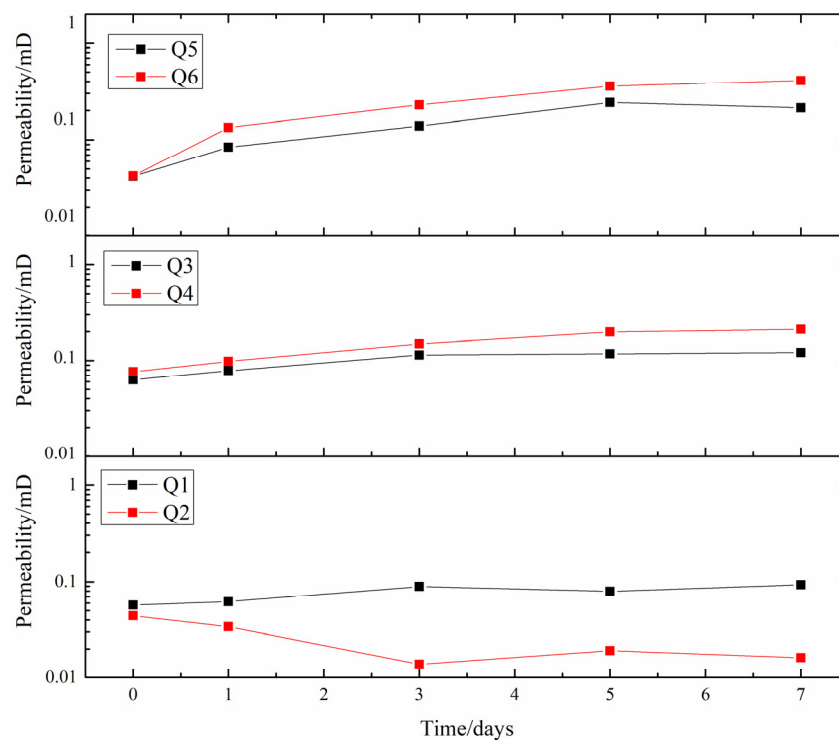


Figure 9. Permeability analysis of shale core samples during CO<sub>2</sub> treatment.

For laminated felsic shale, both porosity and permeability improve significantly after CO<sub>2</sub> treatment. After 7 days' treatment, the porosities of the Q3 and Q4 samples increase by 12.48% and 18.27%, and their permeability increases by 93.31% and 174.97%, both respectively. In combination with SEM analysis, there are many large-sized mineral particles in felsic laminae, such as albite, potash feldspar, calcite and so forth. After CO<sub>2</sub> treatment,

the large-scale dissolution of these minerals occurs and results in many large-sized pores, and the sizes of new dissolution pores can reach 10–30  $\mu\text{m}$  in diameter. Although the precipitation and migration of minerals caused by  $\text{CO}_2$  treatment can partially block pores and throats, the large-scale dissolution effect dominates the change rule, leading to an increase in porosity and permeability. Therefore, it might be better to apply  $\text{CO}_2$  technology for enhancing oil recovery when the target formation mainly consists of laminated felsic shale.

For laminated diamictic shale, both porosity and permeability improve significantly after  $\text{CO}_2$  treatment. After 7 days' treatment, the porosities of the Q5 and Q6 samples increase by 17.68% and 24.78%, and their permeability increases by 412.47% and 872.21%, both respectively. In combination with SEM analysis, besides large-sized feldspar particles, there are many biogenic calcium carbonate minerals. The dissolution effect results in many dissolution pores and dissolution microfractures, which can significantly improve the porosity and pore connectivity of shale. Although the precipitation and migration of minerals caused by  $\text{CO}_2$  treatment can partially block pores and throats, the existence of dissolution pores and fractures dominates the change rule, leading to a dramatic increase in porosity and permeability. When the target formation mainly consists of laminated diamictic shale, the application of  $\text{CO}_2$  technology is recommended. Through the mechanisms of miscible flooding, viscosity reduction, formation energy supplements and improvement in porosity and permeability,  $\text{CO}_2$  technology can effectively enhance shale oil recovery.

#### 4. Conclusions

In this research, the effects of  $\text{CO}_2$  treatment on different lithofacial types of shale have been systematically studied through core observation and XRF analysis, mineral composition analysis, micromorphology analysis and core soaking experiments. The conclusions are as follows:

The shale in the Qingshankou Formation can be divided into three main lithofacial types: foliaceous shale, laminated felsic shale and laminated diamictic shale. These three main types of shale account for more than 90% of the Qingshankou formation and are the main target area in exploration and development thereof. There are significant differences in micromorphologies and pore structures between them. There are relatively more pores with some natural microfractures in foliaceous shale, a few micropores in laminated felsic shale and hardly any micropores in laminated diamictic shale.

After  $\text{CO}_2$  treatment, there are significant differences between the changes in micromorphologies and pore structures among the three main types of shale. For foliaceous shale, many new, small dissolution pores are generated, accompanied by the precipitation and migration of minerals. For laminated felsic shale, large-scale dissolution occurs and results in many large-sized pores (10–30  $\mu\text{m}$  in diameter), which improves the porosity and pore connectivity of the shale samples. For laminated diamictic shale, the dissolution of biogenic calcium carbonate minerals results in many large dissolution pores and dissolution fractures, which greatly improve the porosity and pore connectivity of the shale samples.

Under the effects of mineral composition and micromorphology,  $\text{CO}_2$  treatment has both improving and damaging effects on porosity and permeability for foliaceous shale. When the target formation mainly consists of foliaceous shale, serious consideration should be given to  $\text{CO}_2$  technology to prevent potential reservoir damage. Meanwhile, for laminated felsic shale and laminated diamictic shale, both porosity and permeability improve significantly after  $\text{CO}_2$  treatment. When the target formation mainly consists of laminated shale, the application of  $\text{CO}_2$  technology is recommended.

**Author Contributions:** Conceptualization, H.L. and J.T.; methodology, S.M. and Y.G.; investigation, D.L. and G.C.; writing—original draft preparation, J.T.; writing—review and editing, S.M.; supervision, H.L. All authors have read and agreed to the published version of the manuscript.

**Funding:** This research was funded by the Central Program of Basic Science of the National Natural Science Foundation of China (No. 72088101), the National Key Research and Development Program

of China (No. 2018YFE0196000), and the Foundation Program for Directly Affiliated Institutions of CNPC (No. 2019D-500808).

**Institutional Review Board Statement:** Not applicable.

**Informed Consent Statement:** Not applicable.

**Data Availability Statement:** Not applicable.

**Conflicts of Interest:** The authors declare no conflict of interest.

## References

1. Wang, J.; Feng, L.; Steve, M.; Tang, X.; Gail, T.E.; Mikael, H. China's unconventional oil: A review of its resources and outlook for long-term production. *Energy* **2015**, *82*, 31–42. [\[CrossRef\]](#)
2. Zou, C.; Yang, Z.; Cui, J.; Zhu, R.; Hou, L.; Tao, S.; Yuan, X.; Wu, S.; Lin, S.; Wang, L.; et al. Formation mechanism, geological characteristics and development strategy of nonmarine shale oil in China. *Pet. Explor. Dev.* **2013**, *40*, 15–27. [\[CrossRef\]](#)
3. Wu, T.; Pan, Z.; Liu, B.; Connell, L.D.; Sander, R.; Fu, X. Laboratory Characterization of Shale Oil Storage Behavior: A Comprehensive Review. *Energy Fuels* **2021**, *35*, 7305–7318. [\[CrossRef\]](#)
4. Jin, L.; Hawthorne, S.; Sorensen, J.; Pekot, L.; Kurz, B.; Smith, S.; Heebink, L.; Herdegen, V.; Bosshart, N.; Torres, J.A.; et al. Advancing CO<sub>2</sub> enhanced oil recovery and storage in unconventional oil play—Experimental studies on Bakken shales. *Appl. Energy* **2017**, *208*, 171–183. [\[CrossRef\]](#)
5. Song, Z.; Song, Y.; Li, Y.; Bai, B.; Song, K.; Hou, J. A critical review of CO<sub>2</sub> enhanced oil recovery in tight oil reservoirs of North America and China. *Fuel* **2020**, *276*, 118006. [\[CrossRef\]](#)
6. Alam, M.M.; Hjuler, M.L.; Christensen, H.F.; Fabricius, I.L. Petrophysical and rock-mechanics effects of CO<sub>2</sub> injection for enhanced oil recovery: Experimental study on chalk from South Arne field, North Sea. *J. Pet. Sci. Eng.* **2014**, *122*, 468–487. [\[CrossRef\]](#)
7. Pankaj, P.; Mukisa, H.; Solovyeva, I.; Xue, H. Boosting oil recovery in naturally fractured shale using CO<sub>2</sub> huff-n-puff. In Proceedings of the SPE Argentina Exploration and Production of Unconventional Resources Symposium, Neuquen, Argentina, 14–16 August 2018.
8. Cho, Y.; Eker, E.; Uzun, I.; Yin, X.; Kazemi, H. Rock characterization in unconventional reservoirs: A comparative study of Bakken, Eagle Ford, and Niobrara Formations. In Proceedings of the SPE Low Perm Symposium, Colorado, CO, USA, 5–6 May 2016.
9. Zou, C.; Zhu, R.; Wu, S.; Yang, Z.; Tao, Z.; Yuan, X.; Hou, L.; Yang, H.; Xu, C.; Li, D.; et al. Types, characteristics, genesis and prospects of conventional and unconventional hydrocarbon accumulations: Taking tight oil and tight gas in China as instance. *Acta Pet. Sin.* **2012**, *33*, 173–187.
10. Gupta, I.; Rai, C.; Sondergeld, C.; Devegowda, D. Rock typing in Eagle Ford, Barnett, and Woodford Formations. *SPE Reserv. Eval. Eng.* **2018**, *21*, 654–670. [\[CrossRef\]](#)
11. Fakher, S.; Imqam, A. Application of carbon dioxide injection in shale oil reservoirs for increasing oil recovery and carbon dioxide storage. *Fuel* **2020**, *265*, 116944. [\[CrossRef\]](#)
12. Jia, B.; Tsau, J.-S.; Barati, R. A review of the current progress of CO<sub>2</sub> injection EOR and carbon storage in shale oil reservoirs. *Fuel* **2019**, *236*, 404–427. [\[CrossRef\]](#)
13. Alvarez, J.O.; Saputra, I.W.R.; Schechter, D.S. The Impact of Surfactant Imbibition and Adsorption for Improving Oil Recovery in the Wolfcamp and Eagle Ford Reservoirs. *SPE J.* **2018**, *23*, 2103–2117. [\[CrossRef\]](#)
14. Alvarez, J.O.; Saputra, I.W.R.; Schechter, D.S. Potential of Improving Oil Recovery with Surfactant Additives to Completion Fluids for the Bakken. *Energy Fuels* **2017**, *31*, 5982–5994. [\[CrossRef\]](#)
15. Bikkina, P.; Wan, J.; Kim, Y.; Kneafsey, T.; Tokunaga, T. Influence of wettability and permeability heterogeneity on miscible CO<sub>2</sub> flooding efficiency. *Fuel* **2016**, *166*, 219–226. [\[CrossRef\]](#)
16. Cheng, C.; Ming, G. Investigation of cyclic CO<sub>2</sub> huff-and-puff recovery in shale oil reservoirs using reservoir simulation and sensitivity analysis. *Fuel* **2017**, *188*, 102–111. [\[CrossRef\]](#)
17. Liu, F.; Lu, P.; Griffith, C.; Hedges, S.W.; Soong, Y.; Hellevang, H.; Zhu, C. CO<sub>2</sub>-brine-caprock interaction: Reactivity experiments on Eau Claire shale and a review of relevant literature. *Int. J. Greenh. Gas. Control* **2012**, *7*, 153–167. [\[CrossRef\]](#)
18. Yin, H.; Zhou, J.; Jiang, Y.; Xian, X.; Liu, Q. Physical and structural changes in shale associated with supercritical CO<sub>2</sub> exposure. *Fuel* **2016**, *184*, 289–303. [\[CrossRef\]](#)
19. Yu, W.; Lashgari, H.R.; Wu, K.; Sepehrnoori, K. CO<sub>2</sub> injection for enhanced oil recovery in Bakken tight oil reservoirs. *Fuel* **2015**, *159*, 354–363. [\[CrossRef\]](#)
20. Wei, B.; Zhang, X.; Liu, J.; Xu, X.; Pu, W.; Bai, M. Adsorptive behaviors of supercritical CO<sub>2</sub> in tight porous media and triggered chemical reactions with rock minerals during CO<sub>2</sub>-EOR and -sequestration. *Chem. Eng. J.* **2020**, *381*, 122577. [\[CrossRef\]](#)
21. Lahann, R.; Mastalerz, M.; Rupp, J.A.; Drobniak, A. Influence of CO<sub>2</sub> on New Albany Shale composition and pore structure. *Int. J. Coal Geol.* **2013**, *108*, 2–9. [\[CrossRef\]](#)
22. Lai, F.; Li, Z.; Fu, Y.; Adenutsi, C.D. Investigating the Effects of Pore-Structure Characteristics on Porosity and Absolute Permeability for Unconventional Reservoirs. *Energy Fuels* **2020**, *35*, 690–701. [\[CrossRef\]](#)
23. Xu, T.; Apps, J.A.; Pruess, K. Mineral sequestration of carbon dioxide in a sandstone-shale system. *Chem. Geol.* **2005**, *217*, 295–318. [\[CrossRef\]](#)

24. Steefel, C.; DePaolo, D.; Lichtner, P. Reactive transport modeling: An essential tool and a new research approach for the Earth sciences. *Earth Planet. Sci. Lett.* **2005**, *240*, 539–558. [[CrossRef](#)]
25. Zhang, W.; Yang, W.; Xie, L. Controls on organic matter accumulation in the Triassic Chang 7 lacustrine shale of the Ordos Basin, central China. *Int. J. Coal Geol.* **2017**, *183*, 38–51. [[CrossRef](#)]
26. Zhao, W.; Hu, S.; Hou, L.; Tao, Y.; Xin, L. Types and resource potential of continental shale oil in China and its boundary with tight oil. *Petrol. Explor. Dev.* **2020**, *47*, 1–10. [[CrossRef](#)]
27. Li, J.; Zhou, S.; Li, Y.; Ma, Y.; Yang, Y.; Li, C. Effect of organic matter on pore structure of mature lacustrine organic-rich shale: A case study of the Triassic Yanchang shale, Ordos Basin, China. *Fuel* **2016**, *185*, 421–431. [[CrossRef](#)]
28. Jin, X.; Li, G.; Meng, S.; Wang, X.; Liu, C.; Tao, J.; Liu, H. Microscale comprehensive evaluation of continental shale oil recoverability. *Pet. Explor. Dev.* **2021**, *48*, 256–268. [[CrossRef](#)]